Copy No_____

GENERAL MOTORS CORPORATION

A BROAD SURVEY OF FREE-FLIGHT RANGE MEASUREMENTS FROM THE FLOW ABOUT SPHERES AND CONES

By
R. I. Primich and M. Steinberg

Sponsored by
Advanced Research Projects Agency
U.S. Army Missile Command
ARPA Order No. 347-63

CONTRACT NO. DA-04-495-ORD-3567(Z)
HYPERVELOCITY RANGE RESEARCH PROGRAM

GM DEFENSE RESEARCH LABORATORIES
SANTA BARBARA, CALIFORNIA

TR63-224

SEPTEMBER 1963

A BROAD SURVEY OF FREE-FLIGHT RANGE MEASURLMENTS OF THE FLOW ABOUT SPHERES AND CONES (U)

(Unclassified)

R. I. Primich and M. Steinberg

GM Defense Research Laboratories
Santa Barbara, California

ABSTRACT
(Unclassified)

Free-flight measurements of the flow about both non-ablating and ablating spheres, sphere capped cylinders, and cones are reported. Included are radiometer measurements in the 0.2–5.5 micron band, image converter and schlieren photographs, microwave measurements of wake ionization, head-on radar cross-section measurements, backscatter radar cross-section measurements of turbulent trails, and measurements of precursor ionization. Radiation results for non-ablating spheres, the effect of contaminants, and a comparison between sphere and cone results are presented. The status of the head-on radar results which include anomalous absorption are discussed. Precursor ionization ahead of non-ablating spheres has been identified and attributed to photoionization. Comparative results of both schlieren and radar systems, which involve transition from laminar to turbulent flow and scattering from turbulent wakes are outlined. For cones, conditions cover velocities up to 22,000 ft/sec and pressures up to 150 mm Hg, while for spheres, velocities range up to 24,000 ft/sec and pressures up to 300 mm Hg.

1. TABLE OF CONTENTS

2. INTRODUCTION

A free-flight range is an attractive facility in which to study observables produced by high-speed models because the initial conditions can be carefully controlled, the detection equipment can be placed close to the flight path to yield favorable signal to noise ratios, and not least of all, small-scale experiments can be performed relatively economically. Models are launched at high speed into the free-flight range. There the optical and infrared radiation produced are carefully measured as are the absorption and reflection of microwave signals beamed at the model and at the disturbed flow field. Almost all of the observables encountered in full scale ICBM hypervelocity reentry have been recognized in the laboratory free-flight range. However, the processes which produce the observables do not always scale in a simple way. Recently it has been shown that those processes which depend primarily on two-body collision are scaled when the product of density and model size is preserved.[1] Even where the processes do not scale, the results of model tests are needed to establish the relationships that exist between experiment and our theoretical approximations.

The primary objective of this paper is to present a broad survey of all the programs that are presently being carried out on the Flight Physics Range of the General Motors Corporation. Following a very brief description of the facility and the instrumentation, including the main characteristics, details of the various programs will be presented. In general, familiarity with published

reports will be assumed and only new data not to be found in them will be discussed. Since this is a continuing program most conclusions are tentative, unless otherwise indicated.

3. FACILITY

The free-flight range facility used for the present tests has been discussed by Charters and Curtis[2,3] and will only be summarized briefly here. A light-gas gun launches the model at high velocity into the range proper. The blast chambers isolate the gun from the flight test chamber, so that propellant gases are trapped after the model has passed. In the test chamber, the model velocity is determined by three pairs of stations that accurately locate the model's position and attitude with spark shadowgraph pictures and electronic chronographs triggered by photobeams as the model passes. In the present case when spheres are fired, the model is supported in a plastic sabot while it is being launched from the gun, and the first third of the range is used to separate the sabot from the model. Once separated, the model enters the test chambers where the radiation and microwave measurements are made. The first 75 feet of the free-flight chamber is 2 feet in diameter. The last 50 feet is expanded to 8-feet diameter to minimize wall reflection of radar signals that are beamed along the centerline at the model. The range is sealed so that it may be pumped down to a vacuum, flushed out, and filled with the desired test gas at pressures from 100 microns Hg to atmospheric.

4. INSTRUMENTATION

The flight-range instrumentation and the measurements that can be accomplished with them are conveniently summarized in diagramatic form in Figure 1. They have been described in detail elsewhere[4] and the main features only are outlined here.

4.1. RADIOMETERS[3,4,5,6]

Radiometers have been designed to monitor the emitted radiation from the high temperature flow field. In the case of non-ablating bodies, the main source of radiation is in the stagnation region with less from the flow over the body. An attempt has been made to provide adequate axial resolution to resolve the sources. The viewing area of each radiometer is a rectangular slit with the minimum dimension parallel to the flight axis.

The radiometers used in most of the measurements described here cover the spectral ranges from 0.2 to 0.6 microns, 0.35 to 0.6 microns, 0.35 to 1.0 microns, 2 to 3 microns, 3 to 4 microns, 4 to 5 microns, and 1 to 5.5 microns. The physical arrangements of the photomultipliers for the optical region and the detectors for the infrared region are shown in Figures 2 and 3 respectively. Typical oscilloscope traces obtained with these instruments are shown in Figures 4 and 5. Further details of the apparatus, calibration procedures and data reduction may be found in References 3, 4, 5, 6

The spectral resolution of the radiometers has been recently increased. Eight filter photomultiplier combinations have been installed to monitor the emission in 0.1 micron bandwidths from 0.2 to 1.0 microns. Additional radiometers have been installed to monitor the infrared emission in 1.0 micron bandwidths from 1.0 to 6.0 microns.

4.2. IMAGE CONVERTER CAMERS

An image converter camera has been installed to obtain a photographic representation of the optical radiation emitted by the flow field. Three separate frames each of a few hundred nanoseconds duration and spaced a few microseconds apart are taken. The spectral response is approximately 0.35 to 6.0 microns.

Although quantitative data may be obtained with this device it has been found to be most useful in obtaining rapid information concerning the relative distribution of radiating sources, particularly in comparative studies of ablating and non-ablating bodies.

Some typical results are shown in Figures 6 and 7. In Figure 6 the radiation from the gas cap ahead of a copper-plated sphere is shown. The absence of ablation and wake radiation is self-evident. The radiation from a copper-capped body with a plastic afterbody is shown in Figure 7. Here the gas cap radiation and ablation radiation from the afterbody and the wake can be seen.

4.3. SCHLIEREN SYSTEM

A high-sensitivity, double pass schlieren system,[7] which uses a 10-ft. radius of curvature mirror one foot in diameter is currently in operation. The illumination is obtained with a spark source 15 mil in diameter and having a flash duration of about 200 nanoseconds.

The schlieren system is being used to study details of wake structure (spatial variation of optical refractive index gradients) behind spheres and cones. In particular, emphasis is placed on transitions from laminar to turbulent flow and on structural details of turbulent wakes. In this connection the data is being correlated with similar data obtained by using a high resolution oblique radar (see paragraph 4.5) with the intention of establishing the relationship between" optical" and "electronic" wake structure.

Difficulties have been experienced in the achievement of adequate sensitivity which would reveal wake details immediately behind 5 to 15 mm diameter spheres at conditions under which transition might be expected. In order to improve the sensitivity, a single-pulse laser source has been adapted to a second double pass schlieren system by the Plasma Physics Section of the GM Defense Research Laboratories. The second system employs a 20-ft radius of curvature mirror one foot in diameter. The ruby laser appears to offer a nearly ideal schlieren illumination. Since it emits coherent collimated light, it can be focused to give an extremely small effective source size, thereby increasing the system sensitivity. It can also be operated for very short durations, of the order of 10 nanoseconds. The latter duration produces an extremely small blurred edge on the photograph, only about 0.002 inches at 20,000 ft/sec. More important, however, is the fact that the laser provides a light source of extreme intensity, which is required for the larger schlieren system.

Earlier efforts to use the laser as a schlieren light source have indicated that a very mottled field of illumination is obtained. Current efforts at GM DRL have succeeded in almost eliminating this mottling (see Fig. 8). At the present time, results comparable with those with the more conventional arc source have been obtained. It appears that the laser system is not fully exploited in terms of sensitivity and further improvement can be expected.

4.4. FOCUSED MICROWAVE PROBE[4,8,9]

Arrays of focused microwave beams with good spatial resolution are located across the flight path for the purpose of determining the magnitude and spatial distribution of ionization in the wake. Two frequencies, 35 and 70 Gc, are now in use. The effective spatial resolutions are 1/2 inch and 1/4 inch respectively, and the dynamic ranges are approximately 10^{10} to 5×10^{12} e/cc and 2×10^{10} to 10^{13} e/cc respectively. The idealized disposition of the multibeam system in relation to a typical hypersonic wake is shown in Figure 9. The circles correspond to the effective spatial resolution and contain over 90 percent of the energy in each beam. It should be noted that corresponding beams in the 35 and 70 Gc system provide wake samples at identical radial positions. The 70 Gc probe is used for near wake measurements because of its better resolution, whereas the 35 Gc probe is used for wake measurements.

It has been shown,[4,9] that a good approximation to radial ionization profiles can be obtained by suitably processing the transmission data from adjacent beams. A complex machine program is required which is not yet in use. An example of hand reduction of data in one case is shown in Figure 10. Here the capability of the high resolution probe is fully revealed.

A resonant version of these probes has been developed in prototype form and the results have borne out theoretical predictions that at least two orders of magnitude improvement in sensitivity can be achieved. This instrument will be adapted to range use and is expected to be sensitive to electron densities as low as 10^{8} e/cc. An interesting by-product of this device is that its extreme sensitivity makes it applicable to the measurement of neutral gas density changes.

The conventional probes are described in detail in References 4, 8, and 9 and the resonant probe development is described in Reference 10.

4.5. HIGH RESOLUTION OBLIQUE DOPPLER RADAR

A 35 Gc, CW doppler radar is installed with the beam direction at an angle to the flight path, which can be varied. However, in all measurements to date, the angle has been 45^{0}. In early firings the beamwidth was such that the axial resolution (distance between the first pair of nulls in the antenna pattern) was about 9 inches. This has now been improved by reduction to about 1.5 inches.

This radar is to be used to study backscatter from turbulent wakes. Since the scatter off laminar and turbulent wakes is grossly different it will also be useful in radar studies of wake transition. It is expected that analysis of backscatter records will result in the determination of the properties of turbulent wakes. In all cases the data will be correlated with schlieren data (where possible). An example of the type of record obtained with this radar is shown in Figure 11. In the first photograph the signal from a sphere with no wake can be seen to consist of an envelope which follows the antenna pattern and which contains the individual doppler cycles due to the sphere motion. In the second photograph, of the record from a sphere which is known to have caused a significant (but still underdense) electron wake, the signal which arises from the turbulent wake is clearly visible.

This equipment is still very much in the development stage and a number of modifications and additions are planned. These include (1) a better sensitivity; (2) multi-beam system which will provide a radial resolution capability; (3) electrical recording and (4) at least one additional frequency.

4.6 HEAD-ON CW DOPPLER RADAR

Two radars, which operate at 35 and 70 Gc respectively have been installed on the flight range for the measurement of head-on radar cross section, which is monitored for the last 30 ft. of flight. The purpose of this instrumentation is to study the interaction of the radar waves with the ionization near the body, particularly in the stagnation region.

At the present time the two frequencies cannot be used simultaneously and as a result many firings have to be duplicated. A diplexing system has been developed and will be installed soon. Consideration is being given to the addition of a third frequency of 140 Gc.

Full details of existing equipment are to be found in references 4 and 11.

4.7. PRECURSOR IONIZATION PROBES

Electrostatic probes have been used to monitor electrons ahead of the bow shock wave. These have been described in some detail elsewhere,[12] but, in brief, they are basically flat metallic plates placed normal to the flight line, with provisions made to measure the voltage induced in the plate by the approaching projectile. Various combinations of grids were used in conjunction with the plate to study the effect of body charge and to determine the source of the precursor ionization.

5. DESCRIPTION OF RESULTS

The programs can be conveniently divided into two classes according to the location of the source of observables in the flow field; that is in

1. The Body Flow Field
2. The Wake

5.1. THE BODY FLOW FIELD

In the stagnation region of blunt bodies, intense ionization and radiation are created. In addition precursor ionization may occur due either to photoionization or diffusion. In the case of slender bodies, the stagnation region is not important as a source of observables, but the hot viscous boundary layer appears to result in appreciable radiation and ionization. Significant results which have been obtained in programs designed to study the above observables are now outlined.

5.1.1 RADIATION MEASUREMENTS

5.1.11 NON-ABLATING BODIES

Radiation measurements have been made on 15 mm diameter non-ablating copper-plated spheres over the range of velocities from 13,000 to 22,000 ft/sec and at pressures ranging from 1 to 300 mm Hg. The spectral range from 0.2 to 5.5 microns was covered in bands as described in paragraph 4.1.

Representative plots of the data are presented in Figures 12 to 16 for the spectral regions 0.35 to 0.6 microns and 2 to 3 microns. Figure 12 shows the velocity dependence of peak stagnation emission in the 0.35 to 0.6 micron region for 15 mm diameter copper-clad spheres (non-ablating in air at 10 and 100 mm Hg pressure). At both pressures there appears to be reasonably good agreement with theoretical equilibrium expectations. This is generally the case over the range 0.2 to 1.0 micron at pressures in excess of 10 mm Hg. It should be noted that the equilibrium model is based on a uniform stagnation effective volume of 0.1 r^3 (r nose radius).

The effect of pressure on the 0.35 to 0.6 micron emission is shown in Figure 13. As the pressure decreases below 20 mm Hg, the emission rises relative to the equilibrium expectation. This behavior was observed over the photo-multiplier region from 0.2 to 1.0 micron. The tendency toward increased emission below 20 mm Hg probably results from non-equilibrium gas cap behavior.

Figures 14 and 15 show the velocity dependence of the 2 to 3 micron emission. At 10 mm Hg the experimental results are considerably above equilibrium expectations based on free-free emission calculations but they approach the equilibrium level with increasing velocity. At 100 mm Hg the experimental results are in fair agreement with equilibrium expectations. Similar behavior is noted throughout the range from 1 to 5 microns.

Earlier it was thought that the high emission in the 2 to 3 micron band at the low velocities was due to the 2.7 micron emission from water or OH contamination. Extensive tests with "wet" and "dry" air (laboratory air and cylinder air) have shown this not to be the case. The 10 mm behavior noted in the 2 to 3 micron band in Figure 14 was also observed in the other IR bands which were monitored.

Figure 16 shows the pressure dependence for the 2 to 3 micron emission at 20,000 ft/sec. Here, as in the UV-visible region, there is evidence of non-equilibrium gas cap radiation overshoot as pressure is decreased.

A final word on the influence of water on radiation is in order here. Figures 12 to 16 demonstrate that within the experimental reproducibility of the results there is no difference between the emission from "wet" (up to one percent water) and "dry" (less than 0.1 percent water) air. This appears to be the situation over the spectral range from 0.2 to 5.0 microns.

The simple uniform gas cap model having an effective volume of 0.1 r^3 is actually a very approximate description. Computer codes for gas cap temperature, density, and composition distributions are now in hand at GM DRL and work is in progress to more adequately describe the equilibrium and non-equilibrium gas cap proportions. From these computations a better theory is expected against which the experimental points can be checked.

5.1.12 CONTAMINANT ENHANCEMENT

In a previous report[13] it was shown that Teflon was indeed a low observable ablator. Over the spectral range from 0.2 to 5.0 μ the radiation from the gas cap and wake flow was approximately equal to that from a copper protected model. Polyethylene and Zelux are used often in free flight studies because of the excellent mechanical properties of these materials. With polyethylene, there is a slight enhancement of the gas cap emissivity and a noticeable increase in wake emission. Zelux very strikingly increases the radiative output over the range from 0.2 to 5.0 μ.

Work is continuing on the influence of ablating materials on the observables. Currently an effort is being made to measure the ablation rate of Teflon in free flight through the use of a thin lamina of ablation material marked with strongly luminous sodium on its under side. The time at which ablation uncovers the sodium marker is noted. Success in this venture will permit controlled contamination of wake flows using Teflon as an ablating matrix.

5.1.13 RADIATION FROM NON-ABLATING SPHERES AND CONES

A copper-plated sphere of 7.5 mm radius and 12 1.2° half-angle copper cone of 12-mm base diameter and 1-mm nose radius were fired to obtain a rather graphic comparison of their relative behavior. Radiation measurements were made on the sphere model at an average speed of 18,300 fps for the spectral ranges 0.2-0.6 μ, 0.35-0.6 μ, 0.35-1.0 μ, 2-3 μ, 4-5 μ and 1-5.5 μ. The cone round was fired at a speed of 17,700 fps and radiation measurements were made in the same spectral ranges as for the sphere.

The radiation data obtained for these two models point out in striking fashion the difference between the blunt-nosed and slender-body observables. Both the 7.5-mm-radius sphere and 1-mm-nose-radius cone model are non-ablating configurations. Thus, the radiation may derive from either the gas about the model or from the model surface.

The radiation scope traces (Fig. 17) for the sphere showed a sharp peak of about 2 μsec duration. This corresponds to the transit time of the gas cap through the field of view along the flight line. A second peak about 4 to 5 μsec behind the initial radiation pulse was caused by the recompression shock.

The traces for the cone showed a flat-topped peak corresponding to the transit of the gas cap through the field of view. The pulse was followed by a slowly rising output as the cone (ℓ = 23 mm) passed across the field of view. The output behind the cone fell off quickly. Both models showed little wake radiation except for the recompression behind the sphere. A comparison of the peak outputs from the gas caps of the sphere and cone is given below:

TABLE I. RADIATION INTENSITIES FROM SPHERES AND CONES

Wavelength μ	Peak Intensity, I, in watts/sterad		I Sphere / I Cone
	Sphere	Cone	
0.2 - 0.6[a]	1.6	.009	180
0.35 - 0.6[a]	.25	.0006	400
0.35 - 1.0[a]	.24	.002	120
2 - 3[b]	.214	.010	21
3 - 4[b]	.113	.024	5
4 - 5[b]	.0512	.012	4

a. Field of view along flight line 0.7 cm

b. Field of view along flight line 1.7 cm

If the gas cap radiation were in equilibrium, which is probably not the case for the 1-mm-nose-radius cone, the intensities would vary as r^3, or about 420 to 1. Calculations of heat transfer to the sphere have indicated that body emission is negligible compared with gas-cap emission.[6] Similar analysis have been initiated for conical models.

5.1.2 HEAD-ON RADAR CROSS SECTION MEASUREMENTS

The radar absorption effect for blunt metallic bodies which was first measured in full-scale reentry and which was explained by Musal has been observed in range firings.[11]

Maximum absorption occurs wherever the radar frequency is approximately equal to the plasma frequency in the stagnation region and the thickness of the stagnation plasma is about one half of the freespace wavelength. The plasma thickness in front of small bodies in the flight range is never more than a quarter wavelength (frequencies of 35 and 70 Gc) and the absorption predicted according to the conventional Musal theory is small. However, as has been reported before, (Ref. 11) anomalously large absorption (about an order of magnitude greater) has been measured at both 35 and 70 Gc on copper-capped models with cylindrical after bodies. There has been an element of doubt concerning this type of body, since it is not a complete sphere (which is assumed in the theory) and consequently some peculiar diffraction effect might account for the anomaly. Recent evidence removes this doubt and it is clearly established that the effect is associated with the thin stagnation plasma of a blunt nosed body, and is independent of whether the body is a complete sphere or a spherically capped body.[14]

CARD,[15] has carried out a similar program which incorporated a similar 35 Gc radar and a complete metal sphere of about the same radius as the copper-capped model used here. An anomalous absorption of about the same order has been noted. Also recent experiments[14] at GM DRL with the 70 Gc radar and a 15-mm diameter copper-plated sphere have yielded again anomalous absorption. The results are shown in Figure 18.

Extensive unsuccessful theoretical efforts which were aimed at explaining this phenomena in the free-flight range are summarized in Reference 14. Investigations of additional electromagnetic effects and the possibility of the coupling of EM waves with acoustic waves are continuing.

5. 1. 3 PRECURSOR IONIZATION

Electrostatic probes have been used[12] to determine whether a hypersonic body in flight through the atmosphere accumulates a net charge. In the course of these experiments it became quite apparent that ionization was being created ahead of the bow shock around blunt bodies. Careful experimentation has shown that this is photoionization which probably arises from ultraviolet radiation from the stagnation region. This work has been described in full elsewhere[12] and only the main results will be quoted here.

Figure 19 shows a typical sample of raw data. The rapid increase of induced voltage as the body approaches the probe should be noted. The variation of voltage with distance between the probe and the model is approximately exponential.

The variation of peak voltage (immediately before impact) as a function of velocity is shown in Figure 20, in which a very strong dependence on velocity can be noted. The e-folding distance (of ionization decay ahead of the model) decreases with pressure increase, as would be expected if ultraviolet radiation is supposed to be the source of the ionization.

It was found that the density immediately ahead of the bow shock around a 15-mm diameter sphere fired at 18,000 fps and an ambient pressure of 10-mm Hg was about 10^9e cc. This degree of precursor ionization might be sufficient to account for anomalous radar absorption observed at high altitudes with UHF radar, but not the anomalous absorption discussed in paragraph 5. 1. 2.

Additional experiments are planned in which the effect of body shape will be investigated. Electrostatic probes may be used but emphasis will be placed on the use of the resonant focused

probes which should provide detailed radial and axial distributions of ionization in the precursor region.

5.2. THE WAKE

Wake observables are now of greatest significance since they have the most potential in revealing the vital statistics of the body which causes the wake. Radiation from wakes behind non-ablating spheres or cones has been found to be extremely low intensity. Ablation, however, can appreciably alter this observation. Ionization appears to be present in practically significant quantities in the wakes of both blunt and slender bodies. The details of the wake structure (i.e. laminar or turbulent flow, size and distribution of eddies, etc.) are of major importance in the determination of whether radar backscatter from wakes is measurable or not.

Results of programs which have been carried out to yield basic information in the above areas will be described here.

5.2.1 WAKE RADIATION

5.2.11 BLUNT BODIES

It was stated previously that wake radiation intensities behind non-ablating spheres in the spectral range from 0.2–5.5 μ are very low. In particular, various emitted bands of thermally excited air which have been predicted at times have not been observed. Since the range observations are made with extremely sensitive equipment at a distance of one foot it is likely that this type of radiation would be prominent in full-scale reentry.

Ablation of the body material results in considerable radiation from the wake which depends markedly on the body composition. Preliminary results on the effects of ablation contaminants on wake radiation behind blunt bodies have been reported in Reference 13. Only the main results will be repeated here.

Radiation from Teflon, high-density polyethylene and Zelux (a polycarbonate resin) models was monitored and compared with the radiation from relatively low ablating copper-capped high-density polyethylene models. The velocity range covered was from 12,000 to 24,000 ft/sec in air at 10 mm Hg. The spectral coverage was in seven broad bands from 0.2 to 5.5 microns. The Teflon models showed no enhancement in the spectral range from 0.2 to 5.5 microns. The polyethylene models exhibited appreciable enhancement only in the infrared. Zelux models yielded radiation enhancement throughout the spectrum studied, with relatively larger contributions at longer wavelengths.

Considerable emphasis is being placed on the development of controlled ablation rate techniques. If these are successful it is expected that wake radiation can then be related to the amount of material fed into the wake.

No specific quantitative analysis has been performed on the data obtained with the image converter camera. However, the data has been extremely useful in comparative studies such as the one just described. Examples of the differences in light intensity in the wake from different ablation materials may be found in Reference 13.

5.2.12 CONES

Cone firings are currently in progress and no detailed analysis has been completed. However, a few general comments may be made.

Wake radiation from non-ablating cones (30° to $12\ 1/2^{\circ}$ half angles) is not measurable over a velocity range up to about 20,000 ft/sec and for pressures up to 50–75 mm Hg. Appreciable radiation is observed in the wake for 30° aluminum cones fired at 20,000 to 22,000 ft/sec at 50 mm Hg.

5.2.2 WAKE STRUCTURE

Different instruments can be used to observe different aspects of the wake, all of which have to be combined if a comprehensive wake scattering model is required.

In general the schlieren system is sensitive to transverse gradients in neutral gas density and is thus extremely useful in the detection of the transition from laminar to turbulent flow. It can also be used to yield some information on the size of turbulent eddies. However, since density gradients are integrated along a ray path, caution has to be used in analysing this type of data. Schlieren data can also be useful in the experimental determination of wake velocity.

The structure of the electronic wake is naturally of major interest in any determination of wake radar scattering. The focused microwave probe is sensitive to the mean ionization density throughout the flow field. It can be used to study the spatial distribution of the mean ionization within the probe resolution (1/4" or 1/2"). However, it does not appear to be sensitive to electron density fluctuations characteristic of turbulent media. On the other hand, the backscatter radar, if obliquely oriented to the wake axis, does not detect any backscatter from laminar wakes of almost any mean electron density. As soon as the medium becomes turbulent it is analogous to some degree of "roughness" which causes measurable backscatter.

Initially, measurements of mean electron density in wakes which shed some light on scaling phenomena, effect of contaminants, pressure, velocity, and body shape on ionization will be described. This will be followed by a description of measurements which have been carried out to correlate the optical structure of the wake (as seen by the schlieren) with the electronic structure (as seen by the radar).

5.2.21 MEASUREMENT OF MEAN ELECTRON DENSITY

It was indicated in paragraph 4.4 that radial profiles of electron density throughout the wake may be obtained by routine machine analysis of the data. An example of this type of reduction has been referred to in Figure 10. For many purposes it is much simpler to analyse the data in terms of average electron density. The effective trail diameter at any axial position behind the body can be estimated quite accurately by visual inspection of the data from adjacent probe beams. Since this procedure is quite simple it has been used to obtain all results discussed here.

5.2.211 EFFECT OF CONTAMINANTS ON WAKE IONIZATION

In some early studies of the effect of water vapor on the flow field observables it appeared that about 1 mole percent water almost doubled the electron densities obtained in dry air wakes behind non-ablating spheres and cones. Wake lengths as measured with the transverse probes also increased with the addition of water. The dry air was obtained from cylinders and laboratory air was used for the wet air studies. A dew point cell was used to measure range moisture contents. The dry air firings exhibited excellent reproducibility whereas the wet air firings, under what appeared to be identical conditions, introduced scatter in the transverse probe results.

In subsequent studies to evaluate the "water effect" in detail, cylinder air was bubbled through water to better control the moisture content in the range. Water added in this manner produced results indistinguishable from the dry air results. It appears that the manner in which the range is filled affects the ionization in the wake. Cylinder air is added slowly to the range and atmospheric air is added relatively rapidly. The enhanced wakes observed with atmospheric air now appear to be the result of some other contamination introduced by the stirring up of the inevitably present range debris.

It is interesting to note that the radiation and gas cap properties, as monitored by the head-on doppler radar, were insensitive to the factors which influenced the wake ionization levels. All current and future firings are being made in dry cylinder air.

5.2.212 IONIZATION BEHIND SPHERES AND CONES IN DRY AIR

A fair amount of self-consistent data concerning ionization behind non-ablating spheres in dry air at various velocities and pressures has been obtained. Theoretical calculations for these conditions are planned for comparison. A small sample of this data is shown in Figure 21, where ionization is plotted as a function of distance along the axis for various pressures. Two points should be noted; they are the emergence of the re-compression zone as a function of pressure and the monatonic increase of ionization (at a given axial position) as a function of pressure.

Wake ionization behind ablating aluminum spheres, however, shows markedly different behavior (Fig. 22). Electron densities are considerably greater than for the non-ablating copper-clad spheres. In addition, as pressure is increased, electron density goes through a maximum for any axial distance at about 10 mm Hg. In addition, for a given pressure the electron density reaches a maximum at some axial position. This behavior is obviously quite different from that of non-ablating spheres.

Very few cone firings which were specifically intended as part of an observable program have been completed. Nevertheless sufficient information is available from which an impression of ionization levels behind cones may be formed.

For instance the radiation from a non-ablating cone and sphere under comparable conditions were compared in paragraph 5.1.13. In these firings the ionization immediately behind the sphere is about $10^{12}-10^{13}$ e/cc and that behind the cone is barely perceptible at a level of about $10^{10}-10^{11}$ e/cc. The velocity was approximately 18,000 ft/sec and the pressure 75 mm Hg. Wet (laboratory) air was used. It is found that with dry cylinder air the cone velocity has to be increased to over 20,000 ft/sec before wake ionization is appreciable. To be specific, a 12 1/2° cone (10-mm base radius, 2-mm nose radius), fired at about 21,000 ft/sec into dry air at 50 mm Hg, produces about 10^{13} e/cc immediately behind the base which drops to $10^{10}-10^{11}$ e/cc in less than 15 base diameters. This rapid decay indicates that the flow is dominated by nose bluntness and does not have the true characteristics of slender body flow. Detailed programs are planned in which the effect of cone angle, nose radius, material, velocity and pressure will be explored in a systematic way.

5.2.213 SCALING OF IONIZATION BEHIND NON-ABLATING SPHERES IN AIR

Some experimental evidence has been obtained which indicates that scaling of ionization behind non-ablating spheres in air is possible. Before these data are presented the conditions for validity of scaling are discussed in some detail.

A direct application of free-flight range results can be made to full-scale flight in the regimes governed by appropriate similitude laws. The complexities of chemistry, ionization, and radiation are added to those of hypersonic fluid dynamics when it is desired to simulate the observables of reentry. As the number of interdependent phenomena have grown sharply with the advent of high-speed flight, the number of nondimensional groups has increased to such a point where partial simulation is often the final alternative. The new dimension of complexity introduced by high temperature chemistry evoked an initial reaction of discouragement because chemical equilibria in a dissociating gas have different power dependencies on density.

Chen,[16] has demonstrated that simultaneous scaling of viscous and chemical equilibrium effects is impossible, thereby requiring full-scale flight duplication. Fortunately, the necessity of simulating this combination of effects is infrequently encountered because at the low altitudes required for chemical equilibration of the field, viscosity influences only a negligible portion of the flow. More recently Glick[17] has pointed out that chemical nonequilibrium scaling of hypersonic flows is limited by three-body reactions occurring simultaneously with binary reactions (again because of incompatible density requirements on similitude). It is important to note that the existence of Birkhoff's[18] binary scaling was not denied by anyone; they simply indicated that there are regimes where it was inapplicable. For velocity duplication, binary scaling requires the preservation of $\rho_\infty L$ = constant where ρ_∞ is ambient density and L a characteristic length. Tertiary scaling of the typical atom recombination reactions would require, in addition, the simultaneous maintenance of $\rho_\infty^2 L$ = constant. Therefore, binary reaction similitude (only) is equivalent to inertial-viscous stress similitude through the Reynolds number.

Recent experimental and theoretical studies are continuing to delineate significant regimes of applicability of binary similitude. The pioneering work of Duff and Davidson[19] involving numerical computations of reaction zones behind shock waves in air showed that a relatively large fraction of the nonequilibrium region obeyed binary scaling. This region embraced the famous nitric oxide overshoot first predicted in Reference 19. Nonequilibrium radiation originating at the luminous front was demonstrated by Camm et al[20] to follow binary scaling. A shock tube experiment was the basis of this conclusion. A very comprehensive study of similitude of chemistry in bow shock airflows has been done by Gibson and Marrone[1] by means of numerical computations. They conclude that the flow may approach very far toward equilibrium before binary scaling is nullified. The reverse, three-body reaction rates can be as large as 30% of the forward rates before significant departures occur. Lees[21] has suggested that binary scaling may also be applied to a large portion of the ionization history in a hypersonic wake. The similar regions of wake flows are terminated by 3-body electron attachment to oxygen.

In the present paper further experimental evidence of binary similitude is offered in the form of microwave phase shift measurements of wake ionization obtained with a transverse probe in the physics range at GM DRL.

In an attempt to determine whether scaling of wake phenomena is feasible, attention was directed to ionization data obtained with non-ablating spheres of different sizes fired under different velocity and pressure conditions. In the simplest form of scaling, if the velocity is held constant, the scaling condition is

$$\rho d = \text{constant}$$

where ρ = specie density

d = $2R$

R = nose radius of blunt body

As part of a wake transition study, spheres of 5 and 15 mm diameter were fired at pressures 10 and 30 mm Hg. The scaling condition requires 5 mm diameter spheres at 30 mm Hg. to be compared with 15-mm diameter spheres at 10 mm Hg (i. e. $5 \times 30 = 15 \times 10$).

In both cases, since firings were made at almost identical velocities it was possible to check the scaling.

In scaling, the invariant observable should be $\eta_e \times d$ where η_e is the actual electron density at some point (x/d) in the wake. In practice the total integrated electron density along a wake diameter is measured with the focused probe, that is

$$\phi = 9\pi \times 10^{-14} \lambda \cdot 2\int_0^r \eta_e(\xi)\, d\xi$$

where ϕ = phase shift of transmitted signal (radians)

λ = probe wavelength (cm)

r = wake radius (cm)

ξ = radial distance from wake centerline (cm)

$\eta_e(\xi)$ = electron density at ξ (cm^{-3})

This can be approximated by

$$\phi = 9\pi \times 10^{-14} \lambda (\eta_e)_{av} \delta$$

where $\delta = 2r$ = wake diameter

Now, if it is assumed that ionization scales for two similar bodies of different sizes (e.g.: body diameters d_1 and d_2),

$$d_1 \eta_e(\xi_1) = d_2 \eta_e(\xi_2)$$

at

$$\frac{x_1}{d_1} = \frac{x_2}{d_2}$$

where

$$\frac{\delta_1}{d_1} = \frac{\delta_2}{d_2}$$

and

$$\frac{\xi_1}{\delta_1} = \frac{\xi_2}{\delta_2}$$

The last two conditions follow from the similarity of the wake radial profiles at an invariant value of x/d. Thus

$$\left(\eta_{e_1}\right)_{av} \delta_1 - \left(\eta_{e_2}\right)_{av} \delta_2$$

is equivalent to

$$\left(\eta_{e_1}\right)_{av} d_1 \qquad \left(\eta_{e_2}\right)_{av} d_2$$

at any given value of x/d. Hence, the measured phase shift of the focused probe transmitted beam can be used to check the validity of the scaling relationship.

The quantity $(\eta_e)_{av} \times \delta$ is plotted as a function of x/d for the two sizes of sphere for each of the pressure conditions outlined above.

The comparison between a 5 mm sphere at 30 mm Hg and a 15 mm sphere at 10 mm Hg, is shown in Figure 23. The velocities for the rounds are within 200 fps of each other. The two curves virtually coincide as would be expected if binary and dynamic similitude prevail.

It is not known with certainty whether the wakes described above are either laminar or turbulent since the sensitivity of the schlieren system at that time was not adequate to reveal details of the wake structure. No backscatter returns were observed with the oblique radar which is an indication of the absence of turbulence. Transition data obtained elsewhere also indicates that the wakes should be laminar under the above conditions.[7] Since scaling appears to be practical, the data shown in Figures 23 may be applied to full-scale situations. Suppose that a one-meter diameter sphere be considered. Then the data in Figure 23 would apply to an altitude at which the pressure is

$$p = \frac{5 \times 30}{1,000} = 0.15 \text{ mm Hg}$$

or roughly 200 kft altitude.

The average electron density behind this vehicle would then be obtained from Figure 23.

It should be remembered that scaling has been demonstrated for a size change of three. Certainly, more extensive verification of the similarity considerations demonstrated here will be required before these results can be extended with confidence to full scale vehicles which are 100 times larger than the laboratory models.

5.2.22 MEASUREMENT OF WAKE TURBULENT STRUCTURE

Following a description of some optical and radar observations of the transition from laminar to turbulent flow, further details of measurements of radar scattering from turbulent wakes behind both ablating and non-ablating spheres and cones will be given

5.2.221 TRANSITION FROM LAMINAR TO TURBULENT FLOW

A detailed knowledge of the factors which govern the transition from laminar to turbulent flow as well as the transition distance is essential in determining whether these features are a unique characteristic of the body in question. In addition, since radar will undoubtedly have to be used to identify reentry objects it is of equal importance to establish whether there is a correlation between

the electronic properties of the wake and the more usual fluid properties, such as neutral density.

A comparison of the two schlieren photographs in Figure 24 indicates a marked difference in structure and character between the wake of a sphere and the wake of a cone model at approximately equal speeds and ambient pressures. The most striking difference lies in the high level of density-gradient fluctuations throughout the turbulent portion of the cone wake, as compared with the barely discernible turbulent wake of the sphere. Although it is difficult to assess the turbulent structure directly from schlieren photographs, the presence of what appear to be sonic (or Mach type) disturbances outside the turbulent wake (such as is indicated by Point A on the photograph) is suggestive of a fairly regular pattern in the large-scale fluctuations of the boundary of the cone wake.

The near wake of the cone is laminar, as might be expected, while the sphere wake exhibits turbulence immediately downstream of the neck. The onset of turbulence for the cone is of interest. A small isolated "eddy" (marked Point B in the photograph) is visible before the flow becomes completely turbulent.

Rather intense striae (indicated by Point C), evidently indicative of slip lines originating at the shock front near the body, obscure the details of the near wake of the cone. Hence, no meaningful assessment of the separated flow region or the recompression region can be made from these photographs.

It is evident that the transition details behind a cone are easily studied with the available schlieren system at pressures of interest. On the other hand, because of the very much weaker density-gradient fluctuations behind spheres (as noted above), the study of transition in this case is much more difficult. However, in a few cases, transition behind a sphere appears to have been observed on both the oblique radar and the schlieren systems. A comparison of one of the better schlieren records with the oblique radar record of a comparable round is shown in Figure 25. Here the oblique radar shows no backscatter immediately behind the sphere signal for a distance of about 8 body diameters. An oscillating signal then starts abruptly and is believed to be backscatter due to the onset of turbulence. The periodicity of this signal is believed to be due to the doppler shift arising from the mean fluid motion in the wake (see next paragraph). On the schlieren photograph in Figure 25 the laminar core develops a slight wiggle which goes into a larger amplitude oscillation signalling the onset of turbulence at about 7 body diameters.

Optical and radar transition behind cones has been observed on several firings. Here the correlation is extremely good and the data is easily reproducible. This is believed to be a consequence of the high level of density gradients which exist in the turbulent region behind a cone. A comparison of the schlieren and radar transitions is shown in Figure 26.

5.2.222 RADAR SCATTERING FROM TURBULENT WAKES

5.2.2221 RADAR MEASUREMENT OF WAKE VELOCITY

Since the oblique radar is a CW doppler radar any backscatter signal from wakes should contain information regarding the component of fluid velocity along the direction of the radar beam.

In general, if F(t) is the backscattered voltage received at the radar, then

$$F(t) = A(t) \cos\left(\omega_0 t + \delta(t)\right)$$

This representation is good only if the characteristic fluctuation times of A(t) and $\delta(t)$ are long

compared to the period of ω_0. In the case of the oblique radar in which automixing is used, the output signal is

$$F(t) \sim A(t) \cos \delta(t)$$

Again this representation is good if the characteristic times of A(t) are long compared to those of $\delta(t)$, which in turn have to be long compared to the period of ω_0. If backscattering from a very underdense turbulent trail in which the turbulent fluctuations are small, is considered, then F(t) would resemble an almost periodic signal, in which the mean amplitude would be almost constant and the period would correspond closely to the doppler shift associated with the mean axial fluid velocity.

The data obtained in backscattering measurements of wakes behind spheres and cones has been examined in this way.

In the case of spheres mere visual inspection of the records indicates that the signals are almost periodic. A number of firings have been analysed to obtain the mean fluid velocity. The results are plotted in Figure 27 where they are also compared to the Lees and Hromas theory[22]. The excellent agreement is apparent and it can be concluded that the measured velocity is a mean value associated with a radial position slightly off axis. The results shown in Figure 27 were obtained with the 9-inch resolution system. The more recent 1.5-inch resolution system has provided more exact data, especially in the near wake. In particular, velocities in the recompression zone behind a 15-mm diameter sphere have been resolved. Results for such a case are shown in Figure 28, where the comparison with theory is seen to be excellent.

In the case of cones, the results obtained to date contain a number of inconsistencies. First, for the same firing conditions, non-ablating and ablating cones of the same shape and size do not give the same wake velocity. Ablating cones apparently result in higher wake velocities. Second, a given non-ablating cone fired at different velocities at a given pressure appears to cause different normalized wake velocities (the possibility of ablation setting in at the higher velocities cannot be ruled out). It is quite plausible that these inconsistencies may arise due to the high degree of turbulence which occurs in cone wakes. Because of this it may not be possible to break F(t) down into the approximate form $F(t) \sim A(t) \cos \delta(t)$. In order to investigate this point further, an I. F. system is to be added to the oblique radar. The I. F. will be so high that once again F(t) can be written

$$F(t) \sim A(t) \sin \left(\overline{\omega_i t} \cdot \delta(t) \right)$$

These two signals can be used to find A(t) and $\delta(t)$ unambiguously. It may be found then that the present analysis is faulty in that the so-called doppler signal includes a strong contribution from the turbulent amplitude fluctuations themselves.

5.2.2222 RADAR CROSS SECTION OF TURBULENT WAKES

The oblique radar records of backscatter amplitude have been carefully calibrated and it is possible to assign a radar cross section value to turbulent wakes. This interpretation is of course subject to the correctness of assumptions which are discussed in the previous paragraph. However, for the present it has been assumed that characteristic fluctuation times of A(t) are long compared to $\delta(t)$ and that the measured radar cross section (σ) can be associated with $\overline{A(t)^2}$. According to

one scattering model, the radar cross section per unit volume of wake (δ_v) should depend on the square of the mean electron density within the scattering volume, that is, $\delta_v \propto \overline{\eta}_e^2$

In this theory it is assumed that turbulent scattering arises from a large number of randomly distributed scattering centers, whose characteristic dimensions are small compared to the radar wavelengths. Some firings have been carried out in which all conditions except the water vapor content were held constant. This program was designed to determine the effect of water vapor on mean electron density (See paragraph 5.2.211). As noted there, effects were found which are now attributed to some other contaminant. However, the important point is that a situation arises in which pressure, velocity, and body are fixed but both mean electron density and wake backscatter are varied by the presence of some seeding material. Following suggestions by Salpeter, Treiman, and Lewis[23] this data is being analyzed to check the above theory; that is, the functional dependence of σ_v on $\overline{\eta}_e^2$. Preliminary indications are that the relationship $\sigma_v \propto \overline{\eta}_e^2$ is approached quite rapidly beyond about 40 to 50 body diameters behind the body.

A few cones were fired at that time and, due to the presence of the above contaminant, appreciable backscatter was measured. In one comparison (see Fig. 29) the normalized backscatter from a 12 1 2° non-ablating cone wake was found to exceed that from a non-ablating sphere fired under approximately the same conditions. The mean electron density as actually measured is much greater for the sphere than for the cone. This result is attributed to the greater degree of fluctuation of density behind the cone, but may also be influenced by different scales of turbulence for the two bodies. An additional result is summarized in Figure 30. Here the backscatter and mean electron density behind a 30° ablating aluminum cone are shown. Even though the electron density has fallen well below critical, very large backscatter is noted.

In more recent cone firings, dry air has been used, which has resulted in much lower observables. However, it has been possible to increase the velocity to the point where significant backscatter is observed. An example is shown in Figure 31, where it is evident that measurable backscatter is obtained even though the mean density is not measurable. This example is also of interest in that the radar transition is clearly visible. In the laminar region immediately behind the cone where the mean density is high and measurable no backscatter is observed.

6. CONCLUDING REMARKS

As this is a continuing program, no final conclusions can be reached at this time. Nevertheless, the results which have been obtained show that an integrated free-flight range program can provide information of great value in the understanding of full-scale reentry. The few results which appear to demonstrate the validity of scaling may have far reaching consequences if established over a broader range of parameters. The program which is described here has been two years in the making and has now reached the stage at which a wide category of data is being produced. The accumulation of such data is now expected to accelerate rapidly.

7. ACKNOWLEDGEMENTS

The results reported in this paper are due to the combined efforts of the staffs of the Flight Physics and Microwave Physics Laboratories. Specific contributions to the paper were made by Drs. A.Q. Eschenroeder, C.J. Maiden, L. Wilson, S. Zivanovic, Messrs. R.A. Hayami,

W. Leak, H. M. Musal, Jr., and P. E. Robillard. The laser schlieren was developed by Mr. H. Glenn of the Plasma Physics Laboratory.

8. REFERENCES

1. Gibson, W. E. and Marrone, P. V.: A Similitude for Non-Equilibrium Phenomena in Hypersonic Flight, Paper in AGARD meeting on High Temperature Aspects of Hypersonic Fluid Dynamics. Brussels, Belgium, April 1962

2. Charters, A. C. and Curtis, John S.: High Velocity Guns for Free-Flight Ranges. AGARD paper, Meeting on High Temperature Aspects of Hypersonic Fluid Dynamics, Brussels, Belgium, April 1962. General Motors Defense Research Laboratories. TM62-207

3. Hansen, C. F., Primich, R. I., Steinberg, M. and Maiden, C. J.: Measurement and Analysis of Optical and Microwave Observables in Flow about Hypersonic Models. Paper 63-204, AIAA Summer Meeting, Los Angeles, June 1963

4. Koch, W. L: Instrumentation, Calibration and Data Reduction Methods, GM DRL TR62-213

5. Hansen, C. F. and Leak, W. R.: Equilibrium Stagnation Region Radiation from Pure Air for the 0.2 to 1.0 Micron Band, GM DRL TR62-209F

6. Maiden, C.J. and Steinberg, M.: Infrared Radiation from Low Ablating Hypervelocity Bodies, GM DRL TR62-209G

7. Slattery, R. E. and Clay, W. G.: Measurements of Turbulent Transition, Motion, Statistics, and Gross Radial Growth Behind Hypervelocity Objects, Physics of Fluids, Vol. 5, pp 849-855, 1962

8. Primich, R. I. and Hayami, R. A.: Millimeter Wavelength Focused Probes and Focused Resonant Probes for Studying the Ionized Wakes Behind Projectiles in Free Flight Ranges. Paper at the Millimeter Conference, Orlando, Florida, January 1963 GM DRL TR63-217C, July 1963

9. Primich, R. I. and Hayami, R. A.: Ionization in Hypersonic Wakes. GM DRL TR62-209D, December 1962

10. Primich, R. I. and Hayami, R. A.: The Focused Resonant Probe and its Application to Plasma Diagnostics. Paper at Professional Group (IEEE), Microwave Theory and Techniques Symposium, May 1963, Santa Monica. GM DRL TR63-210, July 1963

11. Musal, H. M., Robillard, P. E., and Primich, R. I.: Radar Absorption Effects Measures in a Flight Physics Range. GM DRL TR62-209B, December 1962

12. Zivanovic, S.: Investigation of Precursor Ionization in Front of the Shock Waves of Hypersonic Projectiles. Paper 63-458 to be given at AIAA Conf. on Physics of Entry into Planetary Atmospheres, August 26-28, MIT, Cambridge, Mass.

13. Steinberg, M., Maiden, C. J., Leak, W. R. and Hansen, C. F.: Preliminary Studies of the Effects of Ablation Contaminants on Radiation. GM DRL TR62-209H, December 1962

14. Musal, H. M.: On the Theory of the Radar-Plasma Absorption Effect. GM DRL TR63-217A, July 1963

15. C.A.R.D.E. Status Report on the Reentry Physics Program. C.A.R.D.E. TM740/63, Apr 1963

16. Cheng, H. K.: Similitude of Hypersonic Real-Gas Flows Over Slender Bodies. J. Aero. Sci. Vol. 26, No. 9, pp. 575-585, September 1959

17. Glick, H. S.: Interaction of Electromagnetic Waves with the Plasmas of Hypersonic Flows, ARS J. Vol. 32, No. 9, pp. 1359-1374, September 1962

18. Birkhoff, G.: Hydrodynamics: A Study in Fact Logic and Similitude, Princeton Univ. Press, Princeton p. 218, 1951

19. Duff, R. E., and Davidson, N.: Calculation of Reaction Profiles Behind Steady State Shock Waves, II. The Dissociation of Air. J. Chem. Phys. Vol. 31, No. 4, pp 1018-1027, October 1959

20. Camm, J. C., Kivel, B., Taylor, R. L., and Teare, J. D.: Absolute Intensity of Non-Equilibrium Radiation in Air and Stagnation Heating at High Altitudes, AVCO Research Report 93, December 1959

21. Lees, L.: Hypersonic Wakes and Trails, ARS Preprint 2662-62, November 1962 (In press for publication)

22. Lees, L., and Hromas, L.: Turbulent Diffusion in the Wake of a Blunt-Nosed Body at Hypersonic Speeds. J. Aero. Sci., Vol. 29, p 976, August 1962

23. Private communication from Salpeter, E. E., Treiman, S. B., and Lewis, H. W.

9. LIST OF FIGURES

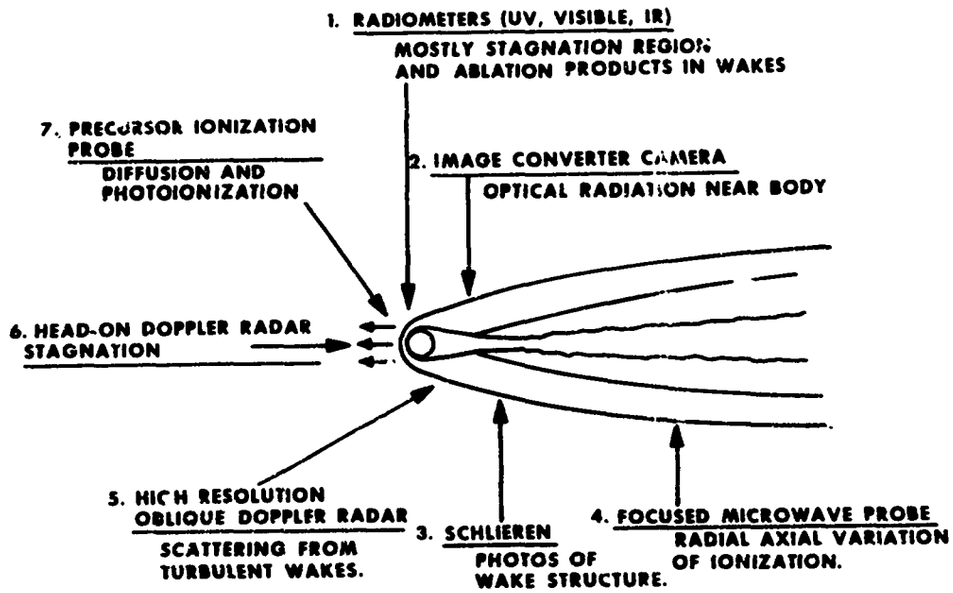

FIGURE 1 MEASUREMENTS ON HYPERSONIC FLOW FIELD

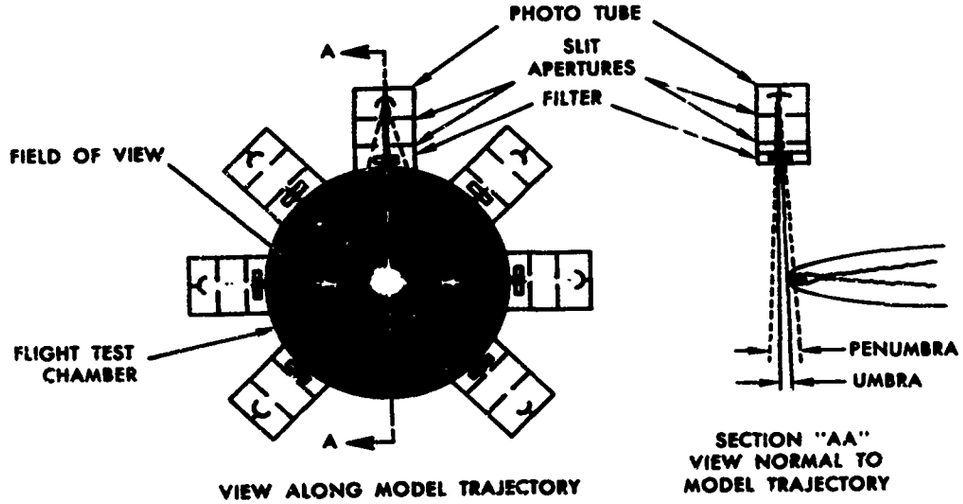

FIGURE 2 PHOTOMULTIPLIER RADIOMETERS

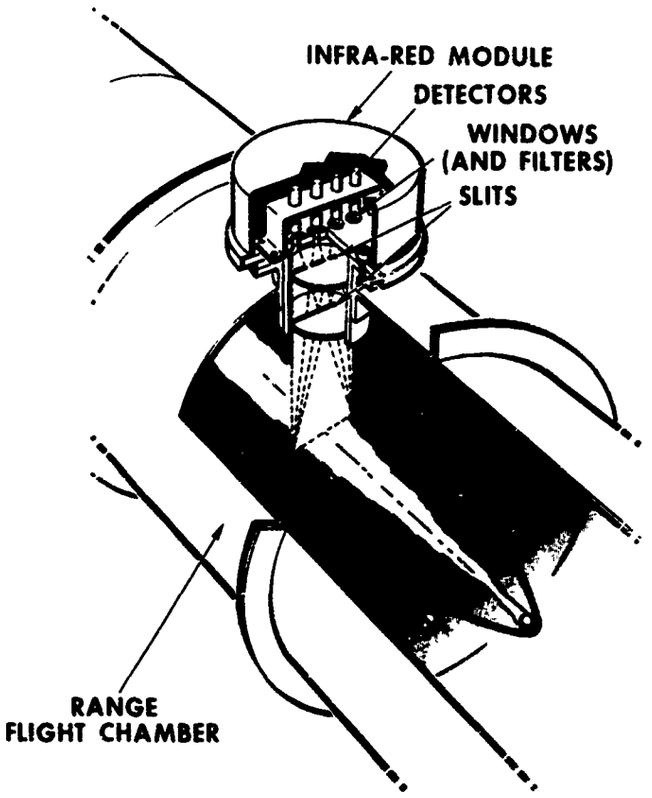

FIGURE 3 INFRARED RADIOMETERS

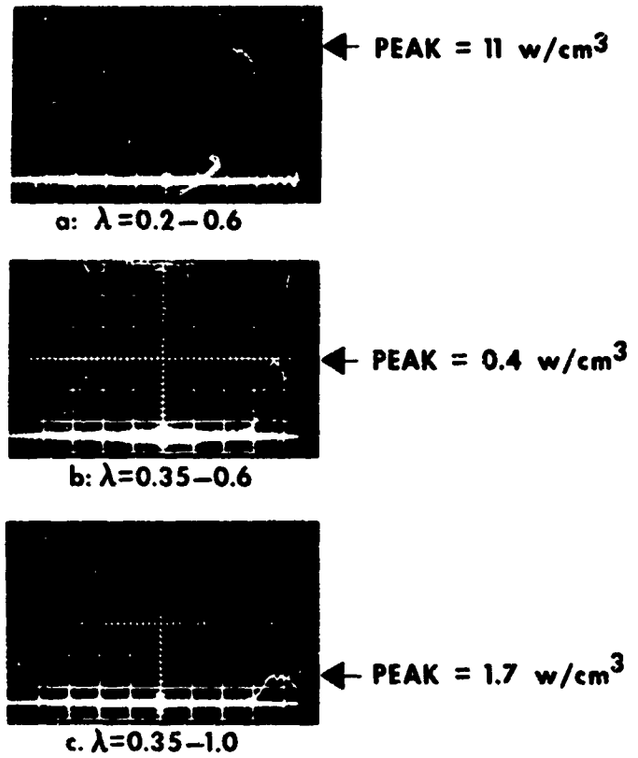

FIGURE 4 PHOTOMULTIPLIER RADIOMETER RECORDS

DETECTOR	BANDWIDTH (MICRONS)	SWEEP SPEED μsec/cm	GAIN volts/cm
A	2–3	5	0.005
B	3–4	5	0.005
C	4–5	5	0.005
D	1–5.5	5	0.05

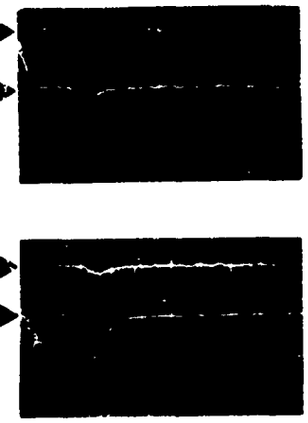

FIGURE 5 INFRARED RADIOMETER RECORDS

FIGURE 6 IMAGE CONVERTER PHOTOGRAPH – NON-ABLATING SPHERE

FIGURE 7 IMAGE CONVERTER PHOTOGRAPH – ABLATING BODY

FIGURE 8 LASER SCHLIEREN PHOTOGRAPH

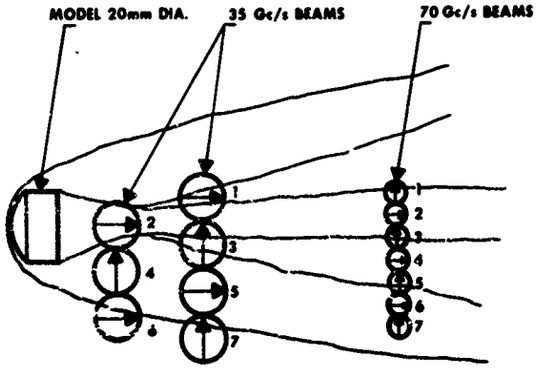

FIGURE 9 DISPOSITION OF FOCUSED MICROWAVE BEAMS ACROSS WAKES

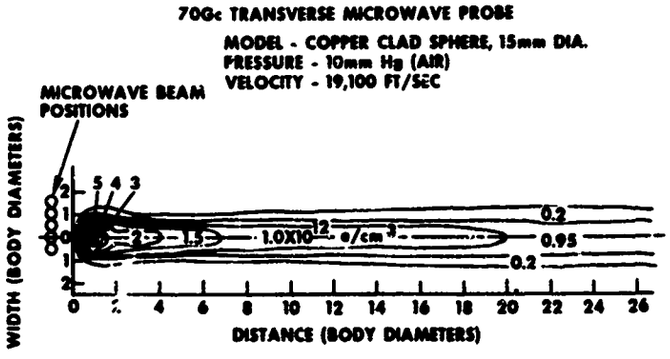

FIGURE 10 ELECTRON DENSITY PROFILES BEHIND SPHERE

15mm DIA COPPER SPHERES AT 20,100 ft./sec

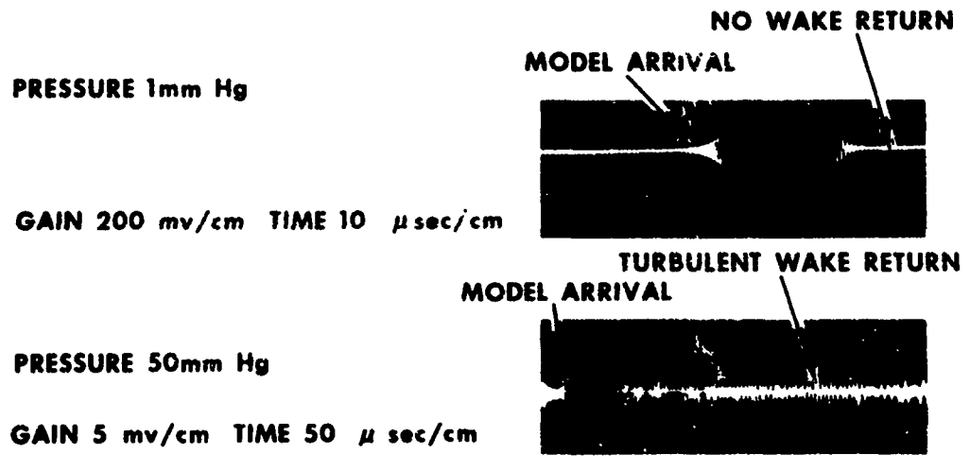

FIGURE 11 OBLIQUE RADAR RECORD

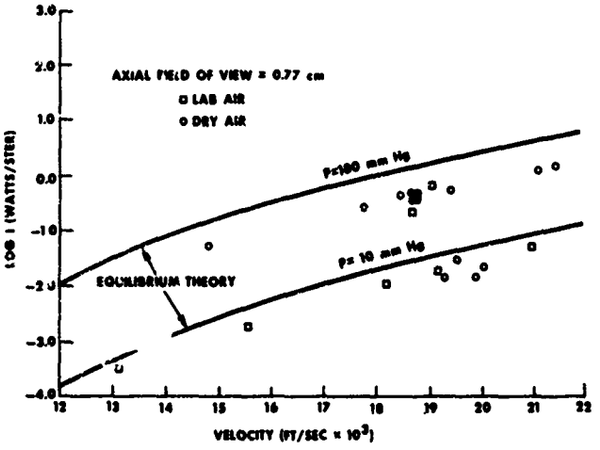

FIGURE 12 VELOCITY DEPENDENCE OF STAGNATION RADIATION, 0.35-0.6μ

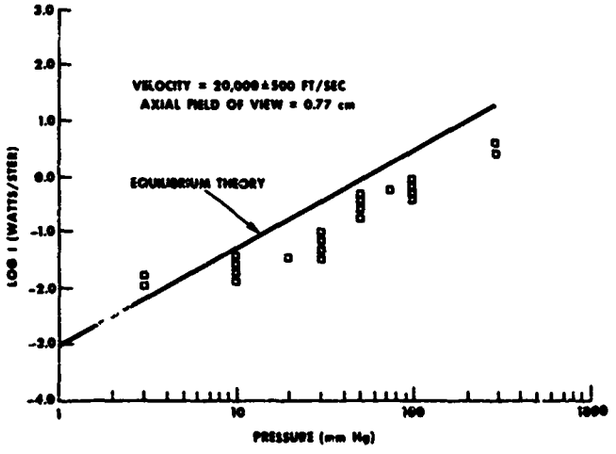

FIGURE 13 PRESSURE DEPENDENCE OF STAGNATION RADIATION, 0.35-0.6μ

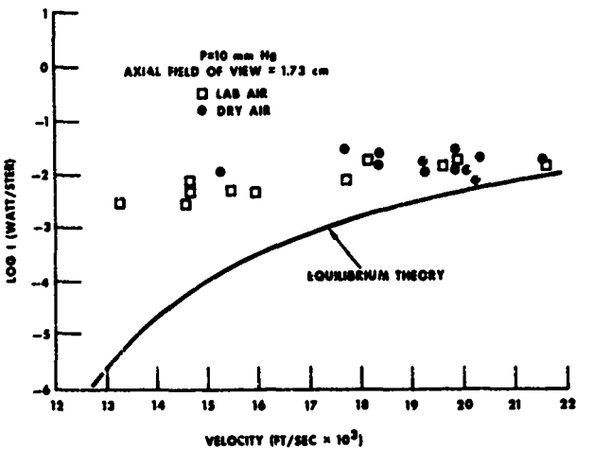

FIGURE 14 VELOCITY DEPENDENCE OF STAGNATION RADIATION, 2-3μ

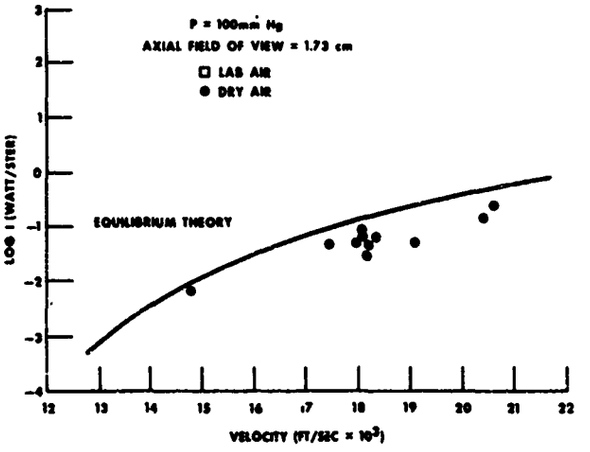

FIGURE 15 VELOCITY DEPENDENCE OF STAGNATION RADIATION, 2-3μ

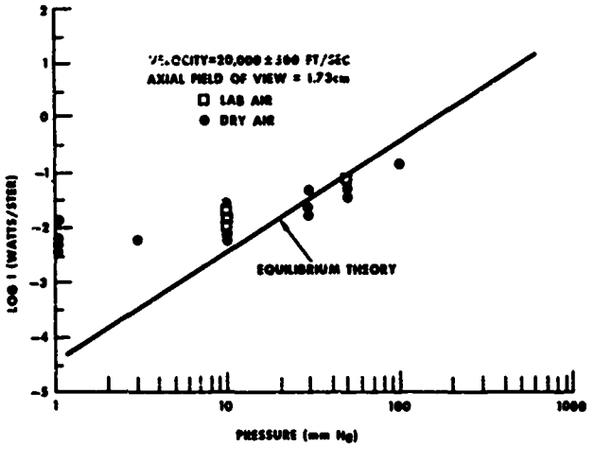

FIGURE 16 PRESSURE DEPENDENCE OF STAGNATION RADIATION, 2-3μ

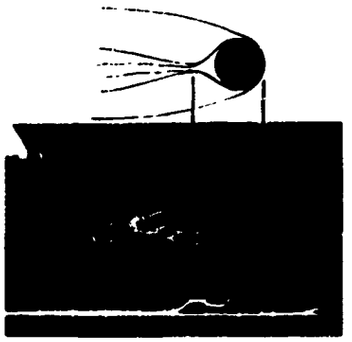

15 mm DIA COPPER SPHERE
VELOCITY= 18,450 fps
SWEEP= 2 μsec/cm
I_{P-AK} = 0.25 WATTS/STER

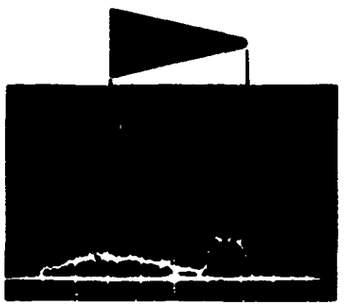

12½° COPPER CONE
NOSE RADIUS= 1mm
BASE RADIUS= 6.25mm
VELOCITY= 17,700 fps
SWEEP= 1 μsec/cm
I_{PEAK} =5.8x10^{-4} WATTS/STER

WAVELENGTH= 0.35-0.6μ
PRESSURE= 76mm Hg

FIGURE 17 SPHERE – CONE RADIATION COMPARISON

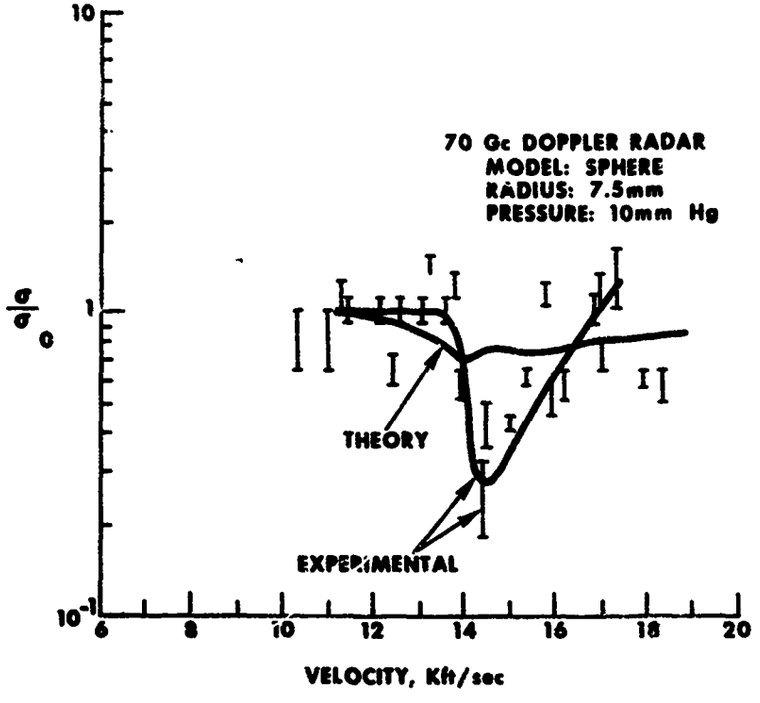

FIGURE 18 RADAR ABSORPTION – COPPER SPHERE

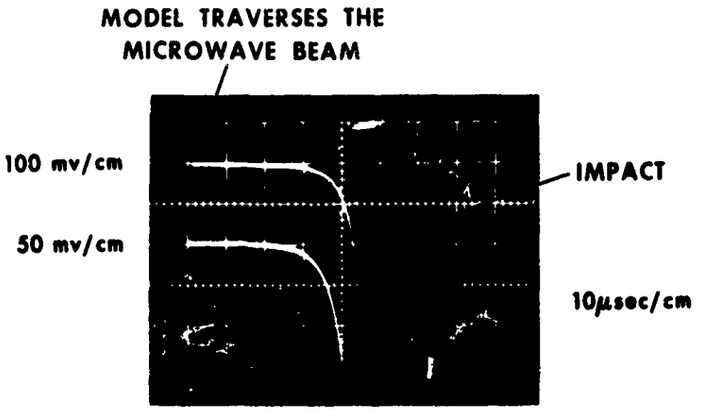

FIGURE 19 TYPICAL PRECURSOR SIGNAL

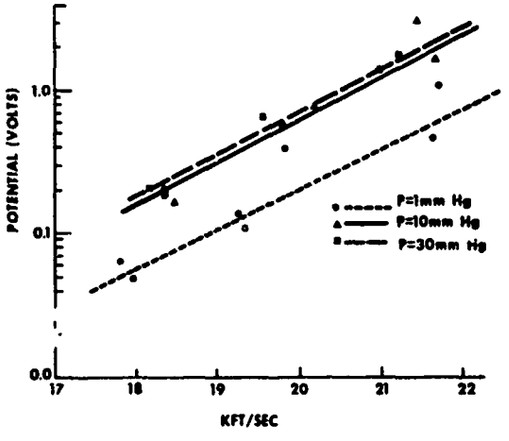

FIGURE 20 PEAK PRECURSOR VOLTAGE VARIATION WITH VELOCITY

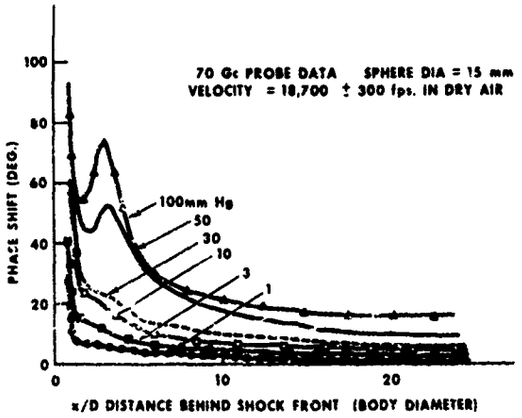

FIGURE 21 NON-ABLATING SPHERE WAKE IONIZATION

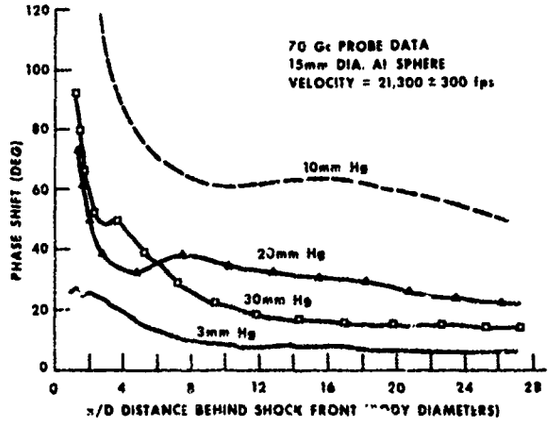

FIGURE 22 ABLATING SPHERE WAKE IONIZATION

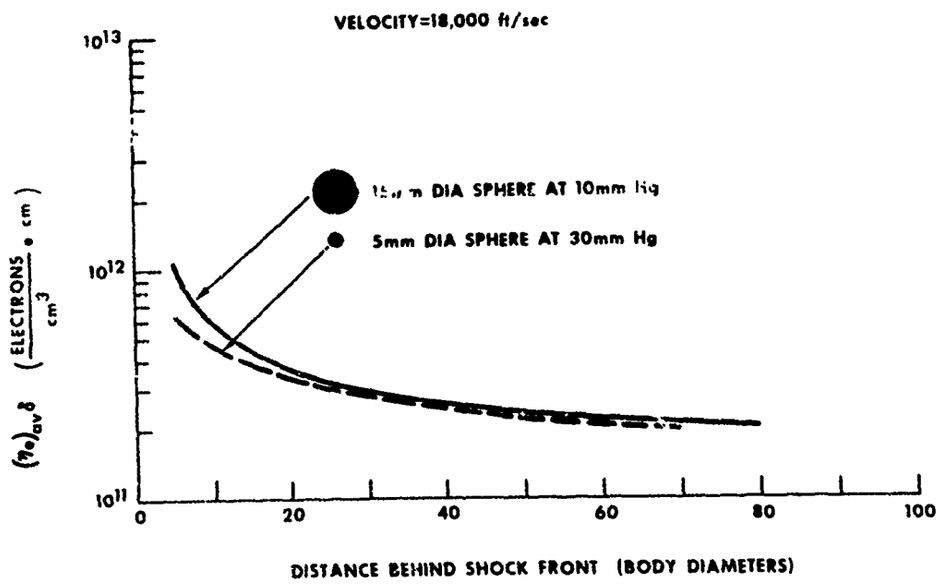

FIGURE 23 WAKE SCALING OF IONIZATION

15mm DIA SPHERE VELOCITY=18,300 ft/sec
PRESSURE=76mm Hg

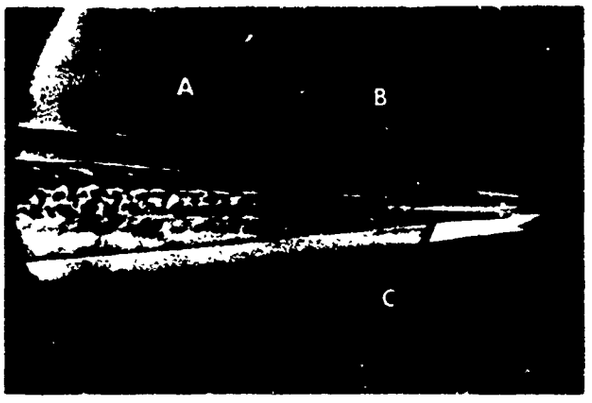

12½° CONE BASE DIA=0.5 VELOCITY=17,700 ft/sec
PRESSURE=76mm Hg

FIGURE 24 SCHLIEREN PHOTOGRAPHS OF CONE AND SPHERE

MODEL=15mm DIA. COPPER SPHERE
PRESSURE=30mm Hg

SCHLIEREN PHOTOGRAPH
VELOCITY=20,700 ft/sec

TRANSITION DISTANCE=7.0 DIAMETER

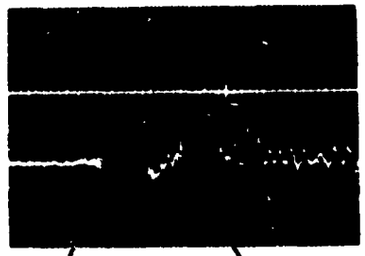

OBLIQUE RADAR RECORD
VELOCITY=19,600 ft/sec
GAIN=10 mv/cm
SWEEP=10 μsec/cm

MODEL ARRIVAL

TRANSITION DISTANCE =8.0 DIAMETERS

FIGURE 25 SCHLIEREN AND RADAR TRANSITION BEHIND SPHERE

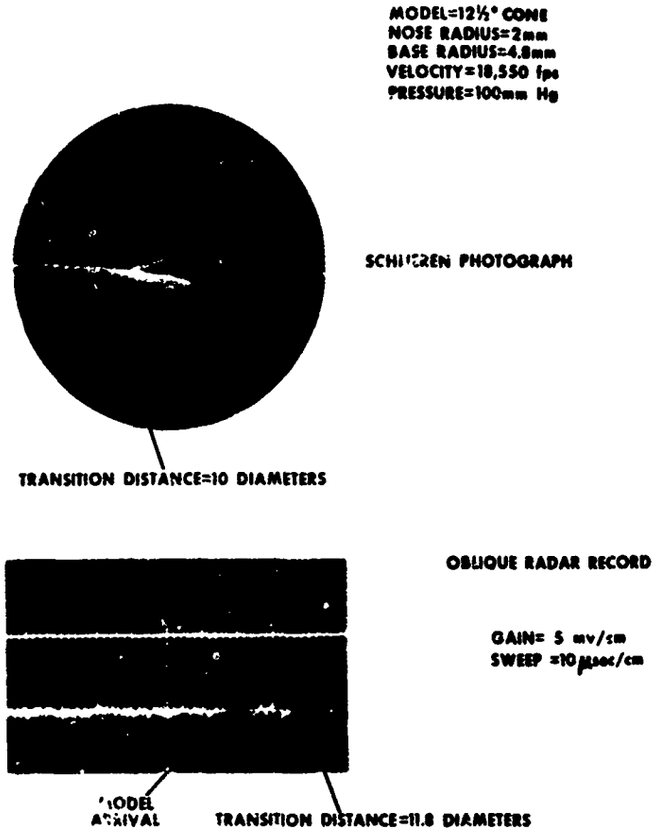

FIGURE 26 SCHLIEREN AND RADAR TRANSITION BEHIND CONE

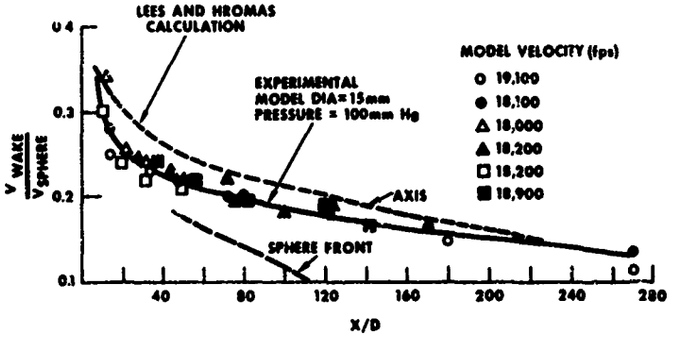

FIGURE 27 WAKE VELOCITIES BEHIND SPHERES

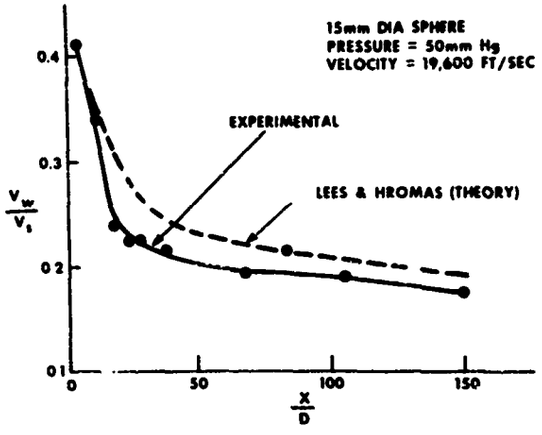

FIGURE 28 WAKE VELOCITY BEHIND A SPHERE

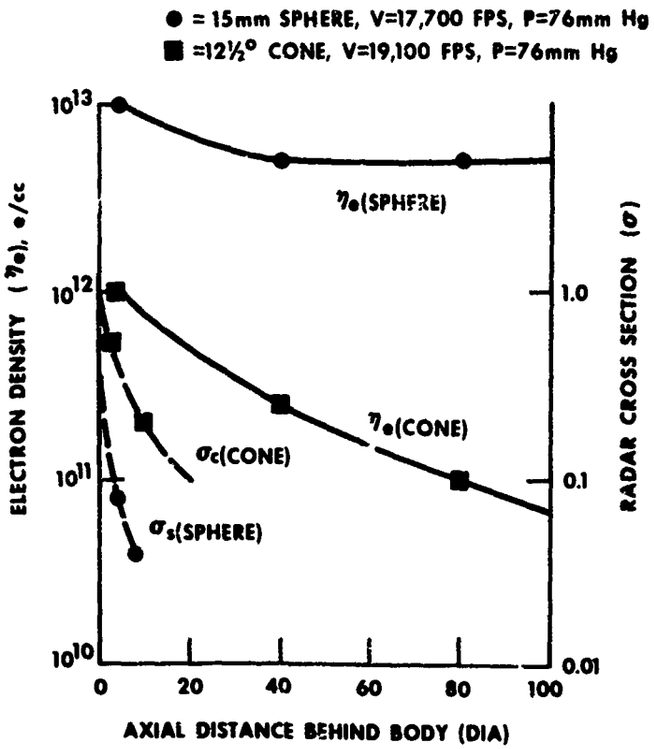

FIGURE 29 BACKSCATTER FROM SPHERE AND CONE WAKES

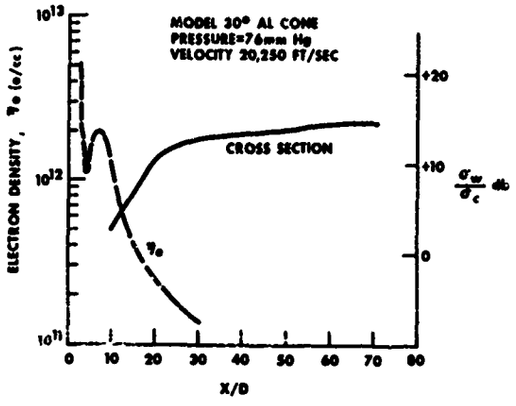

FIGURE 30 BACKSCATTER FROM ABLATING CONE WAKE

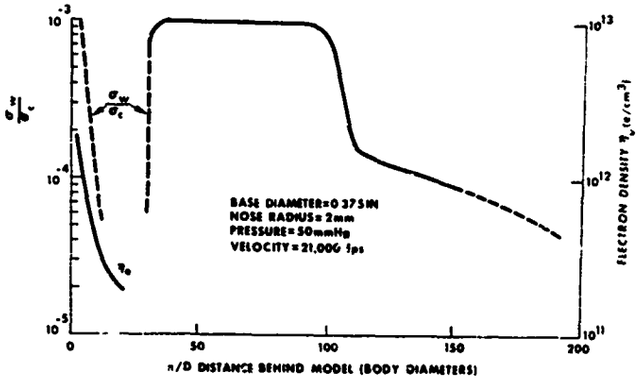

FIGURE 31 BACKSCATTER FROM 12 1/2° C. E WAKE